On Computational Investigation of the Supercooled Stefan Problem

A. Criscione*, D. Kintea, Z. Tuković†, S. Jakirlić, I. V. Roisman, C. Tropea
Institute for Fluid Mechanics and Aerodynamics, Technische Universität Darmstadt, Germany
†Department of Mech. Engineering and Naval Architecture, University of Zagreb, Croatia

Abstract

In the present paper a computational model for the macroscopic freezing mechanism under supercooled conditions relying on the physical and mathematical description of the two-phase Stefan problem is formulated. The relevant numerical algorithm based on the finite volume method is implemented into the open source software OpenFOAM©. For the numerical capturing of the moving interface between the supercooled and the solidified liquid an appropriate level set formulation is utilized. The heat transfer equations are solved in both the liquid phase and solid phase independently from each other. At the interface a Dirichlet boundary condition for the temperature field is imposed and a ghost-face method is applied to ensure accurate calculation of the normal derivative needed for the jump condition, i.e. for the interface-velocity in the normal direction. For the sake of updating the level set function a narrow-band around the interface is introduced. Within this band, whose width is temporally adjusted to the maximum curvature of the interface, the normal-to-interface velocity is appropriately expanded. The physical model and numerical algorithm are validated along with the analytical solution. Understanding instabilities is the first step in controlling them, so to quantify all sorts of instabilities at the solidification front the Mullins-Sekerka theory of morphological stability is investigated.

Introduction

Airframe icing is actually a topic of great importance in the aerospace industry. It is recognized as a significant aviation hazard concerned mainly with the safe and efficient operation of an aircraft under all weather conditions. Large droplets of supercooled water existing in clouds at altitudes which aircrafts have to pass during takeoff and landing procedure impact on the aircraft surface. Consequently the water starts to crystallize ending up with formation of ice. Airframe icing results in increased weight and aerodynamic drag, leading eventually to significant reduction of lift and thrust. In order to maintain public confidence in air transport it is of crucial importance to reduce the rate of occurrence of ice-related incidents. Hence, understanding the freezing process of supercooled water is a problem of fundamental relevance and general utility. The present work aims at a better understanding of thermodynamic processes characterizing the freezing of supercooled water after nucleation with the objective towards improvement of engineering tools for predicting the ice accretion. In the first section of this paper the mathematical description of the physical problem is formulated, whereas the numerical implementation is explained in the second section. The numerical algorithm verification is outlined in the section three. Finally, the most important conclusions are drawn in the fourth section.

Problem Formulation

The process of supercooling occurs when the temperature of a liquid or a gas lowers slowly without external disturbances below its freezing point without turning into solid. Water-to-ice transition under supercooled conditions is considered to be at least a three step process: nucleation, correlative birth of critical nuclei in the whole sample and growth of the macroscopic solid phase. Concerning the last step, closer attention has to be paid to the thermodynamical description of the solidification problem. Two phases are given, a supercooled liquid and a solid phase, and an interface, or a moving boundary, of infinitesimal thickness in between separating the adjacent phases.

Heat Transfer Equations

The starting point is the conservation of mass, momentum and energy:

$$\rho e_t + \rho \vec{U} \cdot \nabla e + p \nabla \cdot \vec{U} = \nabla \cdot (k \nabla T), \tag{1}$$

where ρ is the density, e the internal energy per unit mass, $\vec{U}$ is the velocity vector, p the pressure, k the thermal conductivity and T represents the temperature. Eq. (1) can be simplified as follows

$$\rho c_v T_t + \rho c_v \vec{U} \cdot \nabla T = \nabla \cdot (k \nabla T), \tag{2}$$

*Corresponding author: a.criscione@sla.tu-darmstadt.de

assuming that e depends at most on temperature, the specific heat is constant and the compressibility assumption $\nabla \cdot \vec{V} = 0$ is valid. If neglecting the convective term, Eq. 2 can be further simplified to the following form

$$\underbrace{\rho c_v T_t}_{\rho e_t} = \nabla \cdot (k \nabla T). \tag{3}$$

Interface Condition

At the interface between the liquid and the solid phase an additional condition, the so-called jump condition is needed to close the computational model. Jump conditions for conservative laws can be in general derived as Rankine-Hugeniot shock condition. For a conservation law of the general form

$$D_t + \nabla \cdot \vec{E} = S, \tag{4}$$

the jump condition across a smooth surface, being fixed in space and time, $\xi(\vec{x}, t) = 0$, can be described as follows

$$[D]_{\xi^-}^{\xi^+} N_t + [\vec{E}]_{\xi^-}^{\xi^+} \cdot \vec{N}_x = 0, \tag{5}$$

where $\vec{N}$ denotes the unit vector normal to the surface pointing towards the $+$ side of the interface. Eq. (5) can be expressed as

$$[D]_{\xi^-}^{\xi^+} \vec{v} = \left[\vec{E} \cdot \vec{n}\right]_{\xi^-}^{\xi^+}, \tag{6}$$

where $\vec{v}$ represents the normal velocity of the moving interface

$$\vec{v} := \frac{\vec{dx}}{dt} \cdot \vec{n} = \frac{\vec{dx}}{dt} \cdot \frac{\nabla \xi}{|\nabla \xi|} = -\frac{\xi_t}{|\nabla \xi|}. \tag{7}$$

Introducing these definitions into Eq. (3) and defining the enthalpy jump across the interface as $[\rho e]_{\xi^-}^{\xi^+} = \rho L$, the so-called Stefan Condition follows:

$$\rho L \vec{v} = \left[-k_{\xi^-} \nabla T + k_{\xi^+} \nabla T\right]_{\xi^-}^{\xi^+}, \tag{8}$$

with the indices ξ^- and ξ^+ denoting the solid and liquid phase, respectively. It expresses the local normal velocity of the interface which depends on the heat flux discontinuity at the interface. For the one-dimensional planar solidification of the supercooled water on an ice layer the two-phase Stefan model for a supercooled solidification is to be used. This approach is briefly described in the following section.

Two-Phase Stefan Problem for Supercooled Solidification

The term "two-phase" refers to the phases being "active". Accordingly, both the liquid and the solid phases are active and the heat conservation, Eq. (3), is solved in both. For the derivation of the analytic solution of this problem we consider the one-dimensional case: a semi-infinite slab is occupied by the supercooled liquid at $T_{l0} < T_m$, where T_{l0} is the initial temperature and T_m is the melting temperature of the liquid. At initial time, $t = 0$, a temperature $T_{s0} < T_m$ is imposed at $x = 0$ on the slab (Fig.). Assuming constant densities, $\rho_s = \rho_l := \rho$ and freezing at melting temperature, T_m, the solution for the time-dependent thickness of the solid front $X(t)$ is

$$X(t) = 2\lambda\sqrt{\alpha_s t}, \tag{9}$$

where λ is dependent on the Stefan number [1] and α is the thermal diffusivity. The solution for the temperature in the solid and liquid phase, respectively, is defined as follows

$$T_s(x,t) = T_{s0} + (T_m - T_{s0}) \frac{\left(\frac{x}{2\sqrt{\alpha_s t}}\right)}{erf(\lambda)}, \tag{10}$$

$$T_l(x,t) = T_{l0} + (T_m - T_{l0}) \frac{erf\left(\frac{x}{2\sqrt{\alpha_l t}}\right)}{erf(\nu\lambda)}, \tag{11}$$

where $\nu = \sqrt{\frac{\alpha_s}{\alpha_l}}$.

Interface Condition in Presence of Supercooling

The standard jump condition at the interface, Eq. (8), is valid only for a flat interface at melting temperature, T_m, and constant density. However, in the case of a curved interface the temperature at the interface, T_f, is to be described by the Gibbs-Thomson relation as

$$T_f = T_m \left(1 - \frac{\sigma}{\rho L}\kappa\right) = T_m - \Gamma\kappa, \tag{12}$$

where σ represents the surface tension coefficient, κ is the curvature of the interface and $\rho := \rho_l = \rho_s$. Furthermore, one assumes that the thermal capacity of solid and liquid phases are equal, $c_s = c_l$. The energy conservation across an interface, assuming constant density, is defined by Eq. (3). Assuming that the internal energy $e = h - \frac{p}{\rho}$ the energy jump at the interface can be defined as follows

$$[\rho e]_s^l = \rho \Delta h(T_f) - \left[p_f^l - p_f^s\right], \tag{13}$$

with $\Delta h(T_f)$ representing the enthalpy of fusion. The pressure jump $-\left[p_f^l - p_f^s\right]$, defined by the Laplace-Young relation, is equal to $\sigma\kappa$. Taking into account the Gibbs-Thomson relation, the pressure jump can be described as follows

$$-\left[p_f^l - p_f^s\right] := \sigma\kappa = \rho L \left(1 - \frac{T_f}{T_m}\right) - \rho \underbrace{(c_s - c_l)}_{\Delta c} \left(T_f \ln \frac{T_f}{T_m} + T_m - T_f\right), \tag{14}$$

Accordingly, Eq. 13 may be simplified to

$$[\rho e]_s^l = \rho \left(L - \Delta c[T_m - T_f]\right). \tag{15}$$

For the jump condition being valid for a curved interface we can finally write

$$\rho \left(L - \Delta c[T_m - T_f]\right) \vec{v} = \left[-k_s \nabla T + k_l \nabla T\right]_s^l. \tag{16}$$

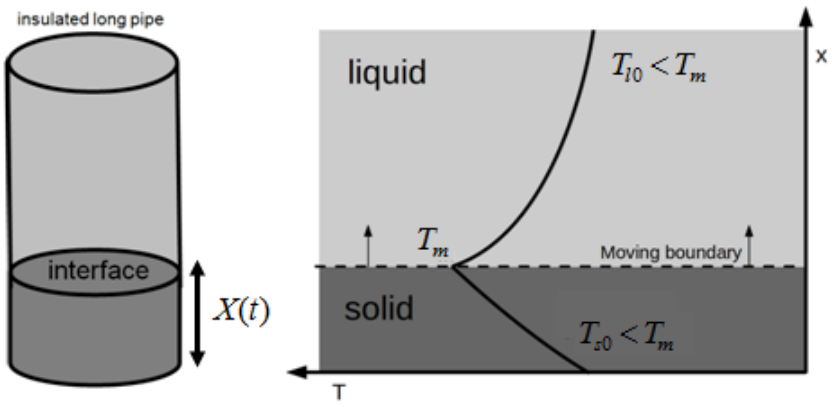

Figure 1. Illustration of a typical temperature profile for the two-phase solidification of supercooled liquid

The Mullins-Sekerka morphological stability analysis

During the solidification of supercooled liquid the interface between the solid and the liquid phase becomes instable because of the destabilizing effect of supercooling, whereas the process described by the Gibbs-Thomson relation acts towards the interface stabilization. The balance between these two effects can be analyzed by the classical approach to morphological stability introduced by Mullins-Sekerka in the context of directional solidification [7, 8]. By utilizing this approach one can study the stability of a flat-interface solution under small perturbations. After perturbations are introduced the interface is defined as follows

$$I(x,t) := \delta(t) \sin \omega x. \tag{17}$$

If the perturbation is small and the interface is kept flat, the approximate solutions of the temperature distribution in the solid phase and the liquid phase take the following form

$$T_s(x,y,t) = T_m + (\nabla T)_s - [\Gamma\omega^2 + (\nabla T)_s]\delta(t), \tag{18}$$

$$T_l(x,y,t) = T_m + (\nabla T)_l - [\Gamma\omega^2 + (\nabla T)_l]\delta(t), \tag{19}$$

respectively. The derivative of the amplitude of the pertubation with respect to time reads

$$\delta'(t) = -\Lambda(\omega)\delta(t), \tag{20}$$

with

$$\Lambda(\omega) = \omega[\Gamma\omega^2(k_l + k_s + V_0\rho\Delta c) + (k_l(\nabla T)_l) + k_s(\nabla T)_s]/\rho L. \tag{21}$$

Where the k stands for the thermal conductivity of the solid or the liquid respectively and V_0 is the interface velocity.

Numerical Procedure

The interface between the solid and liquid phases has to be reproduced correctly. Existing methods for the computation of free surfaces and fluid interfaces can be classified into following two groups [3], namely:

- surface methods (surface fitting) and
- volume methods (surface capturing).

In the first category the interface is represented and tracked explicitly, e.g. by marking it by special marker points [2], or by considering it as a mesh surface which is forced to move with the interface, or by introducing a continuous function over the whole computational domain known as a level set function, which indicates at each point the shortest distance to the surface ([9], [10]). In the second category the fluids are marked by either massless particles (marker and cell method, MAC [5]) or by an indicator function (e.g. Volume-of-Fluid method, VOF [6]).

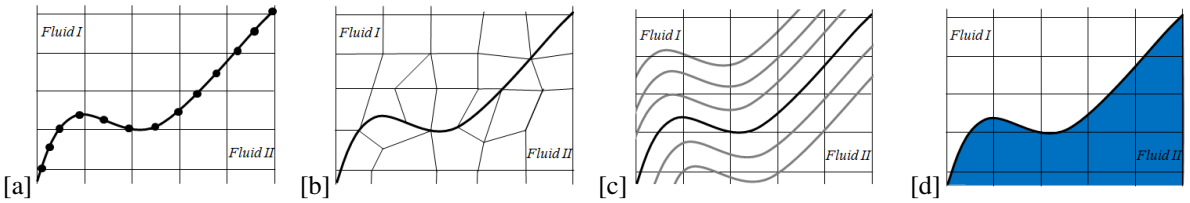

Figure 2. Illustration of different methods for the interface computation - *surface fitting*: [a] Marker points, [b] Interface as mesh surface [c] Level set and *surface capturing*: [d] Indicator function

The advantage of the surface methods is that the interface position is known throughout the calculation remaining sharp as it is convected across the mesh. This facilitate the computational effort needed for the calculation of the interface operations. Contrary, the volume methods have the drawback that the great majority of the convective differencing schemes, which ensure the volume fraction field being within its physical bounds, namely zero and unity, smear the step profile of the interface over several mesh cells. Therefore, in the present work the use of a level set formulation is prefered.

Level Set Approach

The basic idea behind this method is to use an iso-contour of a particular function denoting the surface; the interface is located where this function amounts a certain value [9, 11]. The level set equation

$$\Phi + \vec{W} \cdot \nabla\Phi = 0 \tag{22}$$

is used to keep track of the interface location as the set of points where $\Phi = 0$. The liquid and solid phases are denoted by the points where $\Phi > 0$ and $\Phi < 0$, respectively. Presently, the level set function is defined as a signed distance function. It means the so-called zero level set function describes the interface, whereas the value of the outer level set function represents the distance to the interface whose sign indicates the side of the interface one looks at.

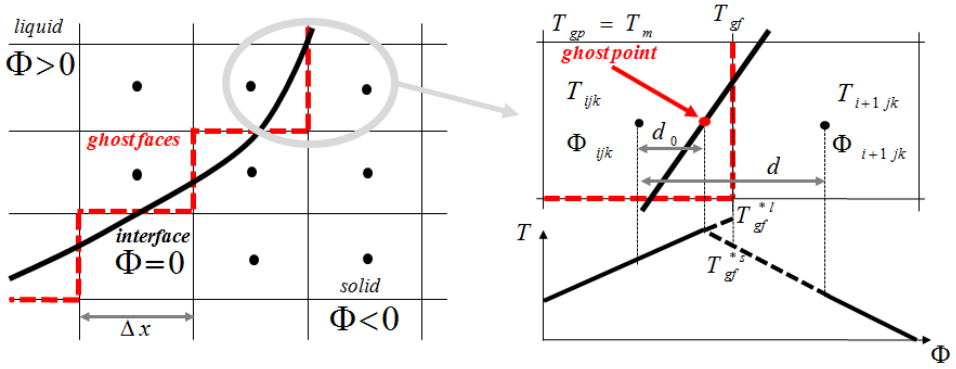

Figure 3. To calculation of the normal temperature derivative at the interface using a ghost face/point method

Dirichlet Boundary Condition imposed at the Interface

The heat transfer equation, Eq. (3), is solved on the subdomain with $\Phi < 0$ independently of the solution procedure for the subdomain where $\Phi > 0$. Hence, two different temperature fields are calculated for the liquid and solid phase, respectively. The temperature at the interface surface, T_i, is imposed as a Dirichlet boundary condition for both temperature fields, in the liquid and in the solid phase.

Interface Velocity

After having calculated the temperature in both subdomains, we use the following procedure to calculate the normal derivative of temperature at the interface. Accurate values of the normal derivative are necessary at grid nodes close to the interface. For this reason ghost-faces are introduced which should separate the liquid subdomain from the solid one, Fig. 3(left). Accordingly, to each individual ghost face in the domain a corresponding ghost point is to be assigned, Fig. 3(right), whose position vector is defined by

$$\vec{C}_{gp} = \vec{C}_{ijk} - \frac{\Phi_{ijk} d}{\Phi_{i+1jk} - \Phi_{ijk}} \frac{\vec{C}_{i+1jk} - \vec{C}_{ijk}}{\left|\vec{C}_{i+1jk} - \vec{C}_{ijk}\right|}. \tag{23}$$

Setting the value of the temperature at all ghost points, $T_{gp} := T_i = T_m$, one may perform a linear extrapolation -from the liquid phase- or interpolation -from the solid phase- for the calculation of the temperature at the ghost face. T^{*s}_{gf} is defined by linear interpolation between T_{i+1jk} and T_{gp}, whereas T^{*l}_{gf} is calculated by linear extrapolation from T_{ijk} and T_{gp}. Now one may calculate the normal derivative $(\nabla T)_n$ close to the interface from the liquid side and that from the solid phase, respectively, using the temperature stored at the cell centers and the calculated values temporarily stored at the ghost face centers. In order to avoid numerical instabilities we expand this procedure with the following restriction: as long as the distance from the grid node P_{ijk} or P_{i+1jk} to the interface is greater than Δx^2 we take T_{ijk} or T_{i+1jk}. Otherwise, T_{i-1jk} or T_{i+2jk} are used instead of T_{ijk} or T_{i+1jk}, [4]. After having calculated $(\nabla T)_n$ at all grid nodes close to the interface the value of the normal derivative at the grid node P_{ijk} is averaged over the belonging phase side of a local running area, Fig. 4 (left). The normal-to-interface velocity, $\vec{v}$, may be estimated in order to fulfill the Stefan condition (Eq. 8). Hence, the interface position changes after each time step; it is evolved in time from Φ^n to Φ^{n+1} using $\vec{v}$ and a first order Euler time-stepping method.

Extension of the Interface Velocity

This makes it necessary to alter the level set function after each time step in order to update it to a signed distance function. This update is done by extending the interface velocity in the normal-to-interface direction within a narrow-band around the interface, Fig. 4 (right). The width of the narrow-band, w_{nb}, is calculated at each time step as

$$w_{nb} = \frac{1}{\kappa^*_{max}}, \tag{24}$$

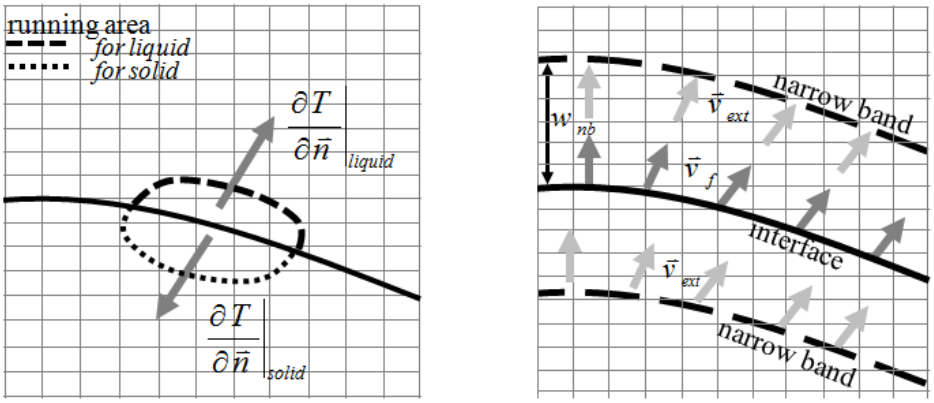

Figure 4. Running average-area of ∇T near the interface for the solid and liquid subdomains (left) and narrow-band method for extension of interface velocity, $\vec{v}_{ext}$ (right)

where κ^*_{max} is the maximum curvature of the interface. The interface velocity is expanded in the direction normal to the interface, $\vec{N} = \dfrac{\Phi}{|\Phi|}$, within the tube on both the liquid and the solid side according to

$$\vec{v}_{ext,t} + \vec{N} \cdot (\nabla \vec{v}_{ext}) = 0, \tag{25}$$

The numerical first-order time discretization given by

$$\frac{\vec{v}^n_{ext} - \vec{v}^{n-1}_{ext}}{\Delta t} + \vec{N} \cdot (\nabla \vec{v}_{ext})^{n-1} = 0, \tag{26}$$

yields

$$\vec{v}^n_{ext} = \vec{v}^{n-1}_{ext} + \vec{N} \cdot \nabla \vec{v}^{n-1}_{ext} \Delta t, \tag{27}$$

Here $\nabla \vec{v}_{ext}$ is discretized locally by a first-order upwind discretization scheme with a propagating direction defined by $\gamma \vec{N}$, where $\gamma = 1$ for the liquid side and $\gamma = -1$ for the solid side. The time step, Δt, is adaptively corrected using the Courant Friedrichs Lewy (CFL) condition, with the Courant number being set to $Co \leq 0.5$.

Update of the Level Set Function within the narrow-band

To retain the values of Φ close to those of a signed distance function ($|\nabla \Phi| = 1$) within the tube, the level set function is updated according to

$$\Phi^n = \Phi^{n-1} - \left(\vec{v}^n_{ext} \cdot (\nabla \Phi)^{n-1}\right) \Delta t, \tag{28}$$

with Δt being also adaptively corrected ($Co \leq 0.5$).

Reinitialization of the Level Set Function

After the update of the level set function within the narrow-band, the outer level set function has to be reinitialized as follows

$$\Phi_\tau + S(\Phi_0)(|\nabla \Phi| - 1) = 0 \tag{29}$$

to enable the setting a new band around the interface in the next time step. Eq. (29) is iterated for a few steps within a fictitious time, τ. $S(\Phi_0)$ is a smoothed-out sign function.

Verification of the Numerical Code

The following chapter is intended to prove that the implemented method is able to handle the Supercooled Stefan Problem in an one-dimensional and a multi-dimensional case.

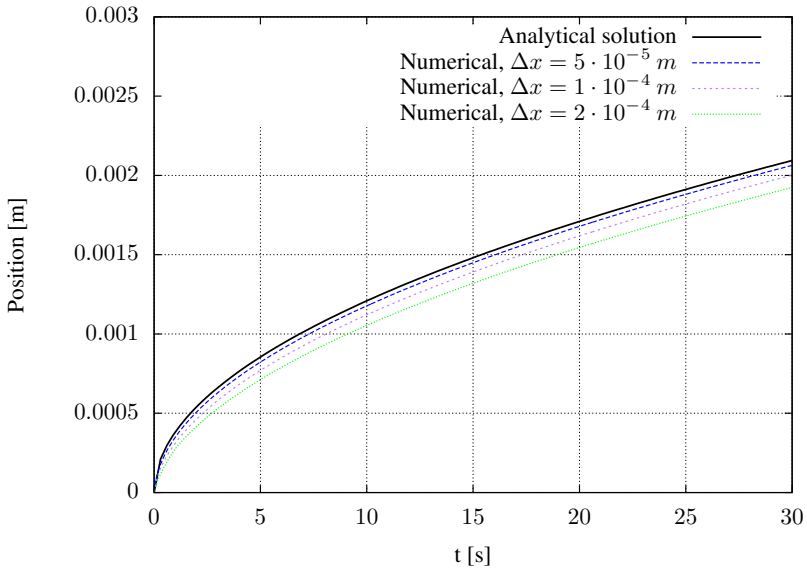

Figure 5. Position of the interface

One-dimensional case

Eq. 9 - 11 are used to verify the numerical code for a supercooled one-dimensional solidification. Let $T_{s0} = T_{l0} = 250K$ and $\alpha_s = \alpha_l = 1.427 \cdot 10^{-7} m^2/s$. The boundary at $x = 0m$ is being held at a constant temperature of $250K$. Fig. 5 shows the position of the interface for different mesh densities. With a decreasing cell size the accuracy of the approximation increases linearly. This shows that the method is converging and is of first order.
In Fig. 6 the numerical approximation for the temperature distribution is shown at $t = 0.5$s and $t = 10$s and compared to the analytic solution which can be described by eq. 10 and 11. The numerical solution has been obtained with a cell size of $\Delta x = 5 \cdot 10^{-5} m$. As it can be seen from Fig. 6 the implemented method is able to approximate the analytical solution very precisely.

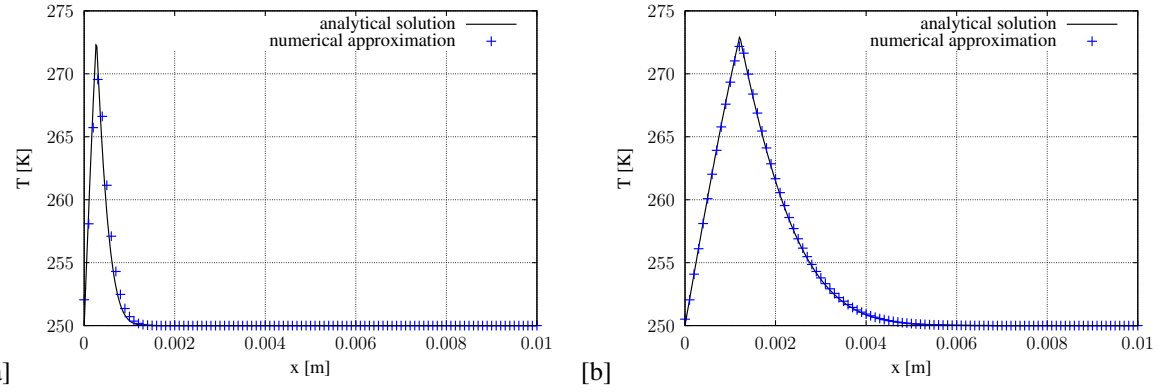

Figure 6. Temperature distribution for two-phase model at [a] t = 0.5s, [b] t = 10s

Two-dimensional case

A study on different alignments of the interface to the mesh, i. e. different angles, has been made to prove the isotropy of the code. The normal vector field in the whole domain has been compared to the ideal normal vector field, which can be obtained from the orthogonal alignment of the interface to the mesh. The greatest observed deviation in the angle of the normal vectors values $0.022°$, which is negligible low for our purposes and occured at an angle of $45°$ between interface and mesh. Therefore the anisitropy of the code can be neglected. For a curved interface we have to validate our numerical code along to the Mullins-Sekerka morphological stability analysis. We introduce a small pertubation describing the interface as defined in Eq. 17, where $\delta(t = 0) = 5 \cdot 10^{-5} m$ and

$\omega = 6283.2m^{-1}$. If there is only a low supercooling of the fluid, the interface is stable, i. e. the amplitude of the pertubation decays exponentially, whereas the amplitude rises if the supercooling reaches a critical value. Such a decay can be seen in Fig. 7 [a]. The figure shows the amplitude of the perturbation over time computed analytically and numerically. Fig. 7 [b] illustrates the exponential growth of the pertubations in case the supercooling is greater than the critical value, i. e. the flat interface is not stable. The increasing deviation between analytical and numerical solution is due to the fact, that one assumption of the analytical solution is that the interface has to remain close to $y = 0$. An increasing deviation of the interface to that value, which is exactly what happens if the amplitudes are growing, will result in an increasing error of the analytical solution. If the frequency of the

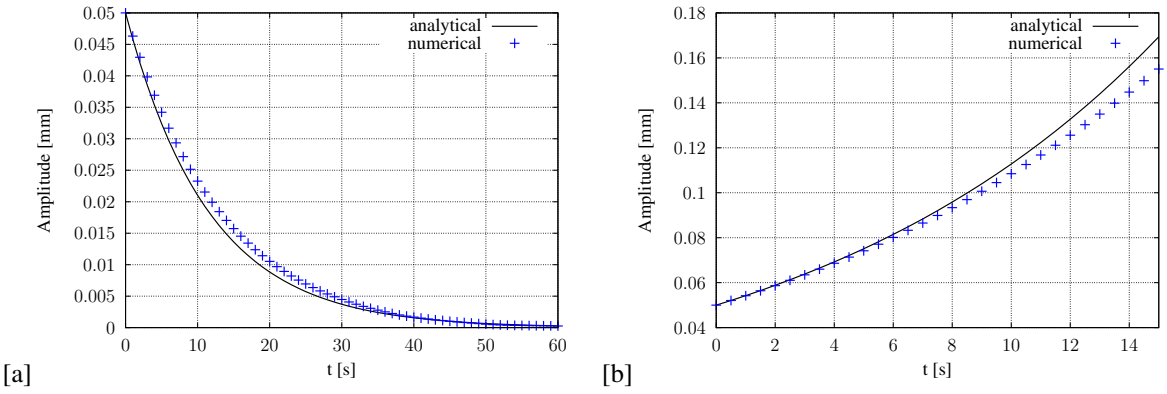

Figure 7. Amplitude of the pertubation

pertubation is raised in the case of an unstable interface it will at some point make the interface stable again, which is a result of the Gibbs-Thomson relation. This effect could be simulated with the described code as well.

Conclusions

We have presented a new level set based algorithm for numerically solving the model equations describing thermodynamical driven processes of the solidification phenomenon of the supercooled water. This algorithm has been implemented into the open source software OpenFOAM©. We have shown excellent agreement between our computations and the theoretical results of Stefan's freezing model. We have quantitatively checked the morphological instability of the pertubated solidification front and compared it against the Mullins-Sekerka theory, obtaining agreement within a few percent. In future work, we intend to introduce kinetic effects resulting from the nucleation step of water-to-ice transition under supercooled conditions into our algorithm.

Acknowledgements

This research was supported by the German Scientific Foundation (DFG) in the framework of the SFB-TRR 75 collaborative research center.

References

[1] Alexiades, V., Solomon, A. D., *Mathematical Modeling of Melting and Freezing Processes* Hemisphere Publishing Corporation, 1993.
[2] Daly, B. J. *Journal of Computational Physics* 4: 97-117 (1969).
[3] Ferziger, J. H., Peric, M. *Computational Methods for Fluid Dynamics* Heidelberg:Springer, 1996.
[4] Gibou, F., Fedkiw, R. P., Cheng, L. T., Kang, M. *Journal of Computational Physics* 176:205-227 (2002).
[5] Harlow, F. H., Welch, J. E. *Physics of Fluids* 8(12): 2182-2189, 1965.
[6] Hirt, C. W., Nichols, B. D. *Journal of Computational Physics* 39:201-225 (1981).
[7] Mullins, W. W., Sekerka, R. F. *Journal of Applied Physics* 34: 323-329, 1963.
[8] Mullins, W. W., Sekerka, R. F. *Journal of Applied Physics* 35: 444-451, 1964.
[9] Osher, S., Sethian, J. A., *Journal of Computational Physics* 79: 12-49 (1988).
[10] Sethian, S. A., *Level set methods; Evolving Interfaces in Geometry, Fluid Mechanics, Computer Vision and Material Sciences* Cambridge University Press (1996).
[11] Sussman, M., Smereka, P. *Computers and Fluids* 27: 663-680 (1998).